Unroofing site-specific α-synuclein–lipid interactions at the plasma membrane

Upneet Kaur[a] and Jennifer C. Lee[a,1]

[a]Laboratory of Protein Conformation and Dynamics, Biochemistry and Biophysics Center, National Heart, Lung, and Blood Institute, Bethesda, MD 20892

Edited by Susan Marqusee, University of California, Berkeley, CA, and approved June 29, 2020 (received for review April 3, 2020)

Parkinson's disease is associated with α-synuclein (α-syn), a cytosolic protein enriched in presynaptic terminals. The biological function of α-syn remains elusive; however, increasing evidence suggests that the protein is involved in the regulation of synaptic vesicle fusion, signifying the importance of α-syn–lipid interactions. We show that α-syn preferentially binds to GM1-rich, liquid-ordered lipid domains on cytoplasmic membranes by using unroofed cells, which encapsulates lipid complexity and cellular topology. Moreover, proteins (Rab3a, syntaxin-1A, and VAMP2) involved in exocytosis also localize with α-syn, supporting its proposed functional role in exocytosis. To investigate how these lipid/protein interactions influence α-syn at the residue level, α-syn was derivatized with an environmentally sensitive fluorophore (7-nitrobenz-2-oxa-1,3-diazol-4-yl [NBD]) at different N- and C-terminal sites. Measurements of NBD fluorescence lifetime distributions reveal that α-syn adopts a multitude of membrane-bound conformations, which were not recapitulated in simple micelle or vesicle models, indicating an exquisite sensitivity of the protein to the complex lipid environment. Interestingly, these data also suggest the participation of the C terminus in membrane localization, which is generally overlooked and thus emphasize the need to use cellularly derived and biologically relevant membranes for biophysical characterization. Collectively, our results demonstrate that α-syn is more conformationally dynamic at the membrane interface than previously appreciated, which may be important for both its physiological and pathological functions.

unroofed cells | GM1 | NBD | fluorescence lifetime

α-Synuclein (α-syn), a widely studied neuronal protein involved in the pathology of Parkinson's disease, remains an enigma because its physiological functions are not well understood (1). α-Syn is concentrated in presynaptic terminals, where it has been proposed to be involved in synaptic vesicle docking, fusion, clustering, and homeostasis (2, 3). As these functions occur on the lipid membrane surface, the ability for α-syn to interact with lipids is essential (4).

Upon membrane binding, α-syn adopts an α-helical structure (5–7), whereas cytosolic α-syn is intrinsically disordered (8). The lipid-binding domain consists of seven imperfect 11-residue repeats that form an amphipathic helix upon membrane association in vitro (9, 10). When membrane-bound, a dynamic equilibrium exists between an elongated helix, encompassing the first 100 residues, and a short N-terminal helix (residues 1 to 25) with a weakly associated unstructured region (residues 26 to 98) (11). While the acidic C-terminal region (residues 100 to 140) remains in solution for both conformations, there is evidence to suggest a functional role for the C terminus as it can bind calcium ions and mediate interactions with SNARE proteins such as VAMP2 (12–14); however, the subcellular spatial context in which this interaction occurs remains unknown. Additionally, a flexible linker region (residues 38 to 44) can be induced by membrane curvature, which gives rise to a broken helix (15–17). While the conformational plasticity of membrane-bound α-syn is proposed to be biologically important (18), direct observation of α-syn conformational heterogeneity at the residue level has yet to be realized on a cellular membrane.

α-Syn–lipid interactions are modulated by lipid composition, membrane fluidity, and curvature (19). Upon binding, α-syn can influence lipid packing within the bilayer (20), induce clustering of vesicles (13), and generate formation of curved lipid structures, such as tubules (21–23) and nanodiscs (24, 25). A large body of work has shown that binding and folding of α-syn are most prevalent when negatively charged, small unilamellar vesicles are present (7, 26–28). Contrary to anionic lipids (29), the protein exhibits the unusual behavior of preferring ordered gel phases of zwitterionic phospholipids in vitro (30, 31), driven by its enhanced affinity for lipid-packing defects (30). This observation is pertinent due to the similarity in the lipid composition to those found in cellular liquid-ordered lipid domains (32), enriched in cholesterol and sphingolipids associated with exocytic sites. However, it remains to be established whether α-syn is found in liquid-ordered lipid domains in vivo (33).

Here, we sought to develop a molecular understanding of α-syn–lipid interactions on cytosolic membranes as related to its biological function. We took advantage of a method called cellular unroofing, which disrupts the upper plasma membrane by brief pulses of ultrasonic vibration, releasing soluble cytoplasmic components, and leaves behind an intact basal membrane (*SI Appendix*, Fig. S1). Using this methodology, numerous vesicular structures and native membrane–protein complexes are preserved along with the cytoskeletal network, achieving the relevant membrane topology of the inner leaflet of the plasma membrane (34). To investigate direct α-syn–lipid interactions on unroofed cells, we employed site-specific Cys variants (V26C, V40C, and Y136C),

Significance

α-Synuclein is a neuronal protein with an ill-defined biological function that is central to Parkinson's disease etiology. While considered to be involved in exocytosis, how α-synuclein facilitates synaptic vesicle fusion and release remains an open question. To address this, we investigated α-synuclein–lipid interactions at the plasma membrane through the technique of cellular unroofing, which uncovers an intact basal membrane. We conclusively show that α-synuclein is recruited to exocytic sites, preferring liquid-ordered lipid domains. Importantly, heterogeneous populations of α-synuclein conformers are revealed by measurements of fluorescence lifetime distributions, which are not adequately described by current models of α-synuclein structures. Membrane-bound α-synuclein is conformationally dynamic, exquisitely sensitive to lipid/protein composition, enabling the protein to carry out its function.

Author contributions: J.C.L. designed research; U.K. performed research; U.K. analyzed data; and U.K. and J.C.L. wrote the paper.

The authors declare no competing interest.

This article is a PNAS Direct Submission.

[1]To whom correspondence may be addressed. Email: leej4@nhlbi.nih.gov.

This article contains supporting information online at https://www.pnas.org/lookup/suppl/doi:10.1073/pnas.2006291117/-/DCSupplemental.

First published July 27, 2020.

which were derivatized with an environmentally sensitive fluorophore, 7-nitrobenz-2-oxa-1,3-diazol-4-yl (NBD) (35). NBD serves as a direct membrane-binding reporter, exhibiting a fluorescence spectral shift with substantially enhanced intensity and lifetime when it is transferred to a hydrophobic lipid environment from a water-exposed state (36–38). In addition, since NBD is weakly emissive in water, there is little contribution from the unbound proteins, minimizing fluorescence background.

We find that α-syn binds preferentially to GM1-rich, liquid-ordered lipid domains, adopting a multitude of conformers at exocytic sites, where SNARE proteins such as VAMP2 and syntaxin-1A reside. Conformational elasticity of membrane-associated α-syn was directly observed on cytoplasmic membranes using NBD lifetime imaging. Interestingly, both N and C termini are involved in membrane localization, experiencing local conformational heterogeneity, which is difficult to reconcile with current structural models of membrane-bound α-syn. By using intact cellular membranes, molecular insights were gained on the dynamic nature of membrane-associated α-synuclein, in which the protein adapts to complex lipid and protein environments in order to carry out its function at exocytic sites.

Results

Unroofed SK-MEL-28 Cells, a Biologically Relevant Membrane Surface. We chose a human melanoma cell line (SK-MEL-28) as a relevant model because it represents a native cellular environment of α-syn as there are high levels of the endogenous protein (39). Moreover, melanocytes are derived from the neuronal crest, sharing many proteins with neuronal cells including those involved in synaptic vesicle homeostasis (40). Representative confocal fluorescence images of an unroofed cell stained with DiD and cholera toxin B (CT-B) are shown in Fig. 1. The lipophilic DiD exhibited a diffusive staining behavior, indicative of an intact phospholipid bilayer (Fig. 1 *A*, *Left*), whereas fluorescently labeled CT-B, a protein that binds to GM1, a ganglioside enriched in lipid rafts (41, 42), showed numerous puncta distributed across the unroofed cell with a low degree of labeling in the surrounding membrane (Fig. 1 *A*, *Right*).

To confirm that the CT-B puncta represented liquid-ordered lipid domains, we performed fluorescence recovery after photobleaching experiments to evaluate fluorophore mobility in the membrane (Fig. 1*B* and *SI Appendix*, Fig. S2). After photobleaching, there was negligible fluorescence intensity recovery observed for regions labeled with CT-B, confirming that these are rigid structures. In contrast, fluorescence intensity fully recovered for regions stained with DiD after 10 s, consistent with a fluid environment as previously reported for unroofed cells (43). This platform retains native-like properties of the inner leaflet of the plasma membrane, composed of fluid and ordered lipids.

α-Syn Is Localized to Liquid-Ordered Lipid Domains on Unroofed Cells. To evaluate α-syn binding to unroofed cells, we first added the most N-terminal NBD-labeled protein at position 26 ($V26C_{NBD}$, 1 μM) due to the strong affinity of the N terminus to bind to lipid membranes (44–46). We note that all proteins herein were expressed as the N-terminally acetylated form as this is a ubiquitous posttranslational modification of α-syn (47). After 5 min of incubation, α-syn is seen in a punctate distribution (Fig. 1*C*), similar to that of the CT-B staining pattern (Fig. 1*A*) with minimal binding to the surrounding membrane areas that are stained by DiD (*SI Appendix*, Fig. S3). As a negative control, we confirmed that the NBD fluorophore did not exhibit an intrinsic affinity for unroofed cells (*SI Appendix*, Fig. S3). A Pearson correlation coefficient (PCC) of 0.56 was found for α-syn colocalization with CT-B, indicating that α-syn prefers liquid-ordered lipid domains (Fig. 1*C* and *SI Appendix*, Fig. S4*A*). This preference was

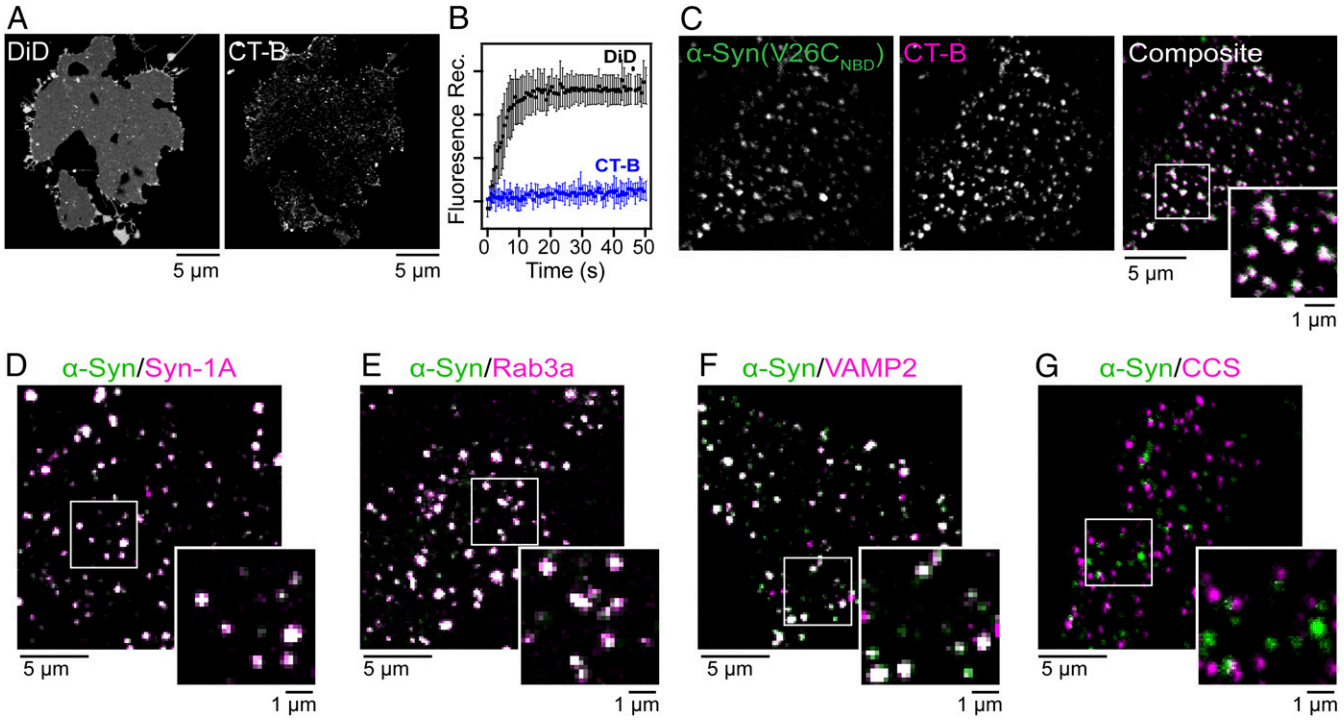

Fig. 1. α-Syn localizes to liquid-ordered lipid domains and exocytic sites on unroofed cells. (*A*) Confocal fluorescence images of DiD- and CT-B–stained unroofed SK-MEL-28 cells. (*B*) Fluorescence recovery traces of DiD (black) and CT-B (blue) after photobleaching. Data are given as mean ± SD ($n = 10$). See *SI Appendix*, Fig. S2 for representative individual region of interest data. Composite confocal fluorescence images of $V26C_{NBD}$–α-syn (green) with (*C*) CT-B (magenta; PCC = 0.56), (*D*) syntaxin-1A (magenta; PCC = 0.77), (*E*) Rab3a (magenta; PCC = 0.88), (*F*) VAMP2 (magenta; PCC = 0.7), and (*G*) clathrin-coated structures (CCS) (magenta; PCC = 0.14). Colocalized areas appear white in the composite images. Expanded views are also shown. Scale bars are as indicated. Additional images can be found in *SI Appendix*, Figs. S4 and S6. Pixel plots for the colocalization analysis can be found in *SI Appendix* Fig. S7.

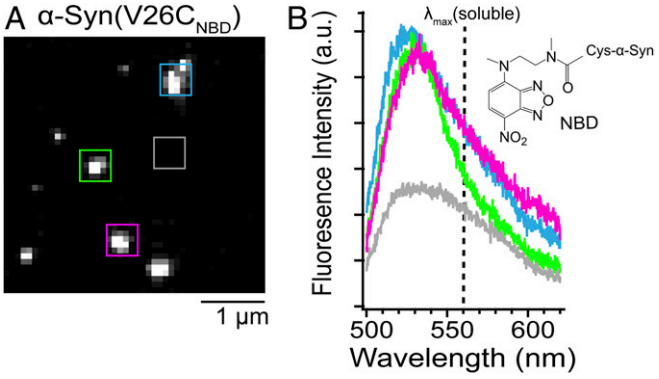

Fig. 2. Spatially resolved fluorescence spectra of α-syn bound to unroofed cells. (*A*) Wide-field fluorescence image of V26C$_{NBD}$-α-syn on unroofed SK-MEL-28 cells. Scale bar is as indicated. (*B*) Fluorescence spectra taken at spatial locations indicated by the colored boxes in *A*. The gray box indicates a background spectrum. For comparison, the dashed line represents the emission maximum (λ_{max} = 555 nm) of V26C$_{NBD}$–α-syn α-syn in solution. (*Inset*) Chemical structure of NBD. See *SI Appendix*, Fig. S8 for additional images and spectra.

verified for endogenous α-syn (*SI Appendix*, Fig. S5*A*). Next, we showed that α-syn also is found in specialized membrane microdomains enriched in gangliosides (e.g., GM1 and GM3) such as caveolae (48, 49). Utilizing an antibody for caveolin-1, a scaffolding protein of caveolae (49), again a high degree of colocalization (PCC = 0.60; *SI Appendix*, Fig. S4*B*) was observed, supporting the finding with CT-B. As a control, a C-terminal Cys-variant (Y136C) labeled with DyLight488 exhibited identical behavior (*SI Appendix*, Fig. S4 *C* and *D*), verifying that the α-syn colocalization pattern on unroofed cells was independent of fluorophore type and labeling position.

α-Syn Is Localized to Exocytic Sites on Unroofed Cells. Since α-syn is proposed to be involved in exocytosis, we tested for colocalization of α-syn (V26C$_{NBD}$, 1 μM) with SNARE proteins, syntaxin-1A (target plasma membrane-associated) and VAMP2 (vesicle-associated) as well as a key exocytosis regulatory protein, Rab3a (50). Colocalization analysis of α-syn with syntaxin-1A (Fig. 1*D*), Rab3a (Fig. 1*E*), and VAMP2 (Fig. 1*F*) resulted in PCC values of 0.77, 0.88, and 0.70, respectively. Endogenous α-syn colocalization at exocytic sites was also verified (*SI Appendix*, Fig. S5*B*). The lower PCC value observed for VAMP2 in comparison to Rab3a and syntaxin-1A is because some fraction of VAMP2 is cargo material within clathrin-coated structures (CCS) (51), where we observe no colocalization of α-syn (Fig. 1*G*; PCC = 0.14). The high degree of colocalization exhibited by α-syn with proteins involved in exocytosis strongly supports that α-syn is recruited to regions involved in exocytic vesicle fusion. Because exocytic regions are enriched in cholesterol, GM1, and PtdIns(4,5)P_2 (52), these colocalization results are consistent with that of CT-B, a specific marker for GM1.

Fluorescence Imaging Spectroscopy Confirms Direct α-Syn–Lipid Interactions. While fluorescence intensity-based images are spatially informative, they do not conclusively show direct protein–lipid interactions. Thus, we turned to fluorescence imaging spectroscopy to obtain emission spectral information at defined locations. Coupling a spectrograph to an inverted microscope, NBD fluorescence spectra of individual α-syn puncta on unroofed cells were measured (Fig. 2 and *SI Appendix*, Fig. S8). As expected, a large spectral blue shift (emission maxima [λ_{max}] = 527 ± 4 nm) was observed compared to that of a water-exposed NBD (λ_{max} = 555 nm; see below), indicating the fluorophore is in a more hydrophobic lipid environment, showing specific interaction of α-syn with the membrane. Interestingly, slight variations of λ_{max} were observed, hinting at the existence of distinctive environments at individual locations. These results show that NBD is a useful reporter of α-syn localization and provides direct evidence of N-terminal α-syn binding to the inner leaflet of the plasma membrane.

Site-Specific α-Syn–Lipid Interactions Revealed by NBD Fluorescence. To develop a molecular understanding of how α-syn binds to biological membranes, conformational changes were evaluated using additional NBD variants (Fig. 3*A*). As a reference, we first characterized α-syn interactions with lysophosphatidylcholine (LPC) micelles and vesicles composed of DOPC/GM1. We chose PC because it is the most common lipid type in mammalian cells, and GM1 was selected because α-syn colocalized with GM1-containing areas on unroofed cells. Circular dichroism (CD) spectroscopy verified that all NBD variants adopted similar secondary structure as the wild-type protein in solution and in the presence of increasing micelles and vesicles with comparable binding affinities, indicating no effect by the NBD fluorophore (*SI Appendix*, Figs. S9*A* and S10).

In solution, all three NBD variants exhibited identical λ_{max} at 555 nm, characteristic of water-exposed fluorophores (Fig. 3*B* and *SI Appendix*, Fig. S9*B*). Both V26C$_{NBD}$ and V40C$_{NBD}$ spectra shifted to 533 nm in the presence of LPC micelles as the fluorophore partitions into the hydrocarbon acyl chains. Similarly, their spectra (λ_{max} = 530 nm) indicated NBD insertion into DOPC/GM1 vesicles, in accord with the elongated helical model (53). Interestingly, the spectrum of Y136C$_{NBD}$ blue-shifted

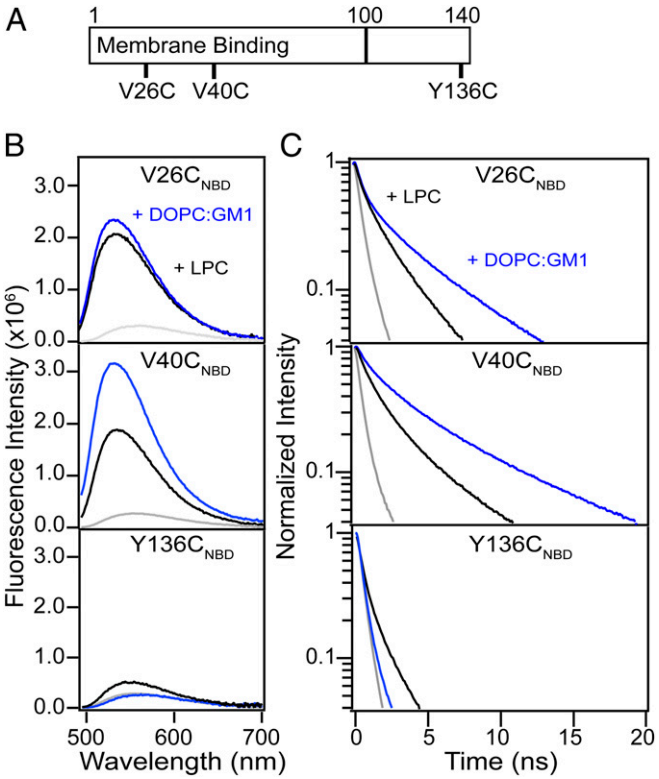

Fig. 3. Site-specific NBD fluorescence of α-syn variants. (*A*) Schematic representation of the α-syn primary sequence. Membrane binding region (residues 1 to 100) and cysteine-labeling sites used in this study (V26C, V40C, and Y136C) are indicated. Comparison of steady-state fluorescence (*B*) and decay kinetics (*C*) of V26C$_{NBD}$ (*Top*), V40C$_{NBD}$ (*Middle*), and Y136C$_{NBD}$ (*Bottom*) α-syn (1 μM) in buffer (gray) and in the presence of either LPC micelles (black; 5 mM) or DOPC/GM1 vesicles (blue; 1 mM). See *SI Appendix*, Tables S1 and S2 for fit parameters.

(λ_{max} = 542 nm) in the presence of LPC micelles, showing interaction of the acidic tail with zwitterionic lipids. This observation is consistent with a previous proposal that the glutamate-rich C-terminal region (residues 120 to 140) interacts with the positively charged choline head groups (54). In contrast, no discernible changes were measured in the presence of the negatively charged GM1 lipids due to electrostatic repulsion, indicating that interaction between the C-terminal tail and the membrane mimics is modulated by specific lipid composition and not driven by the fluorophore.

NBD decay kinetics revealed site-dependent differences (Fig. 3*C* and *SI Appendix*, Fig. S11). Decay kinetics were adequately fit to a double- or triple-exponential function, and the values are reported in the *SI Appendix*, Tables S1 and S2. For simplicity of discussion, only average fluorescence lifetimes (τ_{avg}) are compared. As expected, all variants had relatively short and similar lifetimes in their disordered soluble states (τ_{avg} = 0.5 to 1.0 ns; *SI Appendix*, Fig. S9*C*). Upon micelle and vesicle binding, their lifetimes increased, reflecting a dramatic change in local environment and conformation. Interestingly, differences in the N-terminal region are seen, where position 40 has a higher sensitivity toward lipids (LPC: V40C_{NBD} [τ_{avg} = 3.8 ns] > V26C_{NBD} [τ_{avg} = 2.6 ns]; DOPC/GM1: V40C_{NBD} [τ_{avg} = 6.3 ns] > V26C_{NBD} [τ_{avg} = 4.8 ns]), which we attribute to differences in insertion depths and/or restricted motion when embedded in the lipid acyl chains. These results are in accord with the observed higher overall V40C_{NBD} emission intensity. The near twofold longer τ_{avg} observed for the N-terminal sites compared to that of micelles suggests a more rigid polypeptide conformation upon insertion into the lipid bilayer, similar to previously reported trends using Trp mutants, where N-terminal sites are sensitive probes of α-syn–lipid interactions (44). Consistent with the steady-state data, a longer lifetime for Y136C (τ_{avg} = 1.2 ns) was observed in the presence of LPC micelles, again indicating interaction of the C terminus with zwitterionic lipids. Together, our results demonstrate that NBD is an excellent site-specific probe of α-syn membrane interactions.

Site-Specific Conformational Heterogeneity of α-Syn on Unroofed Cells. Since fluorescence decay kinetics (i.e., lifetimes) can reveal conformational differences of the membrane-bound α-syn populations that are not apparent from intensity-based analyses, we used fluorescence lifetime imaging microscopy (FLIM), a time-resolved image acquisition method to provide information on fluorescence lifetime distributions of NBD variants at different spatial locations on unroofed cells (Fig. 4*A*). Here, the contrast of the fluorescence image is based on the lifetime of individual fluorophores rather than their emission intensity.

Consistent with the intensity-based confocal fluorescence images (Fig. 1*C*), lifetime images of V26C_{NBD}, V40C_{NBD}, and Y136C_{NBD}, displayed distinct punctate patterns on unroofed cells. However, each spot now exhibits a range of colors, representing the measured NBD lifetime per pixel from orange-to-green-to-cyan, spanning 5.5 to 2.5 ns (Fig. 4*A* and *SI Appendix*, Figs. S12–S14), where the τ_{avg} becomes shorter progressing from N-to-C sites, with the N terminus exhibiting the greatest sensitivity.

The fluorescence lifetime distributions (Fig. 4*B* and *SI Appendix*, Figs. S12–S14) of the three NBD-labeled variants indicate that each residue is in a hydrophobic environment as the lifetimes are longer than that measured for soluble α-syn (τ_{avg} = 0.5 to 1.0 ns). V26C_{NBD} exhibits the broadest lifetime distribution spanning from 2 to 7 ns, which is well described by two Gaussian functions with peak maxima centered at 3.2 and 4.6 ns, indicating at least two different conformers (Fig. 4 *B*, *Left*). While they are similar, the maxima do not align exactly with the measured τ_{avg} values of 2.6 and 4.8 ns for micelle- and vesicle-bound V26C_{NBD}, respectively (Fig. 4 *B*, *Left*), suggesting that the

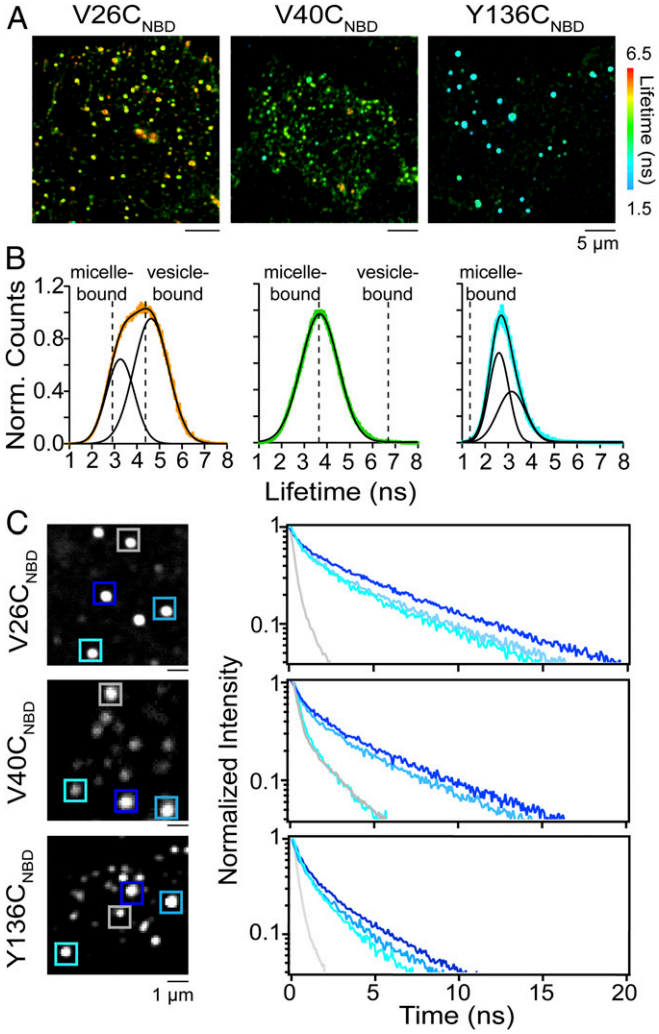

Fig. 4. Site-specific α-syn conformational heterogeneity on unroofed cells revealed by FLIM. (*A*) Confocal fluorescence lifetime images of V26C_{NBD}, V40C_{NBD}, and Y136C_{NBD} α-syn on unroofed SK-MEL-28 cells. Red-to-cyan color scale spans lifetimes of 6.5 to 1.5 ns. (*B*) Fluorescence lifetime distributions of V26C_{NBD} (orange; 14,918 events from n = 46), V40C_{NBD} (green; 11,989 events from n = 30), and Y136C_{NBD} (cyan; 12,823 events from n = 35), where n represent the total number of unroofed cells from two biological replicates. The solid black lines represent Gaussian fits with χ^2 values of 0.26 (V26C_{NBD}), 0.17 (V40C_{NBD}), and 0.24 (Y136C_{NBD}). The dashed lines indicate τ_{avg} values obtained in the presence of LPC micelles and DOPC/GM1 vesicles. For comparison, single Gaussian fits for V26C_{NBD} and Y136C_{NBD} are shown in *SI Appendix*, Fig. S15. (*C*) NBD fluorescence decay kinetics of individual puncta for V26C_{NBD} (*Top*), V40C_{NBD} (*Middle*), and Y136C_{NBD} (*Bottom*). NBD decay kinetics were measured at locations indicated by colored boxes (*Left*). For fit parameters, see *SI Appendix*, Table S3. See *SI Appendix*, Figs. S12–S14 for additional lifetime images, distributions, and decay kinetics.

conformational space that V26C_{NBD} samples is different from the two putative membrane-bound α-syn structures, the broken vs. elongated helix.

In contrast, the distribution of V40C_{NBD} fits well to a single Gaussian function centered at the micelle-bound τ_{avg} value of 3.8 ns (Fig. 4 *B*, *Middle*). Notably, V40C_{NBD} exhibits shorter lifetimes than V26C_{NBD}, opposite to the trend characterized in either presence of lipid micelles or vesicles. Despite being only 14 residues apart, their behaviors are distinct on unroofed cells and not easily explained by the available structural models (9, 15, 55). For Y136C_{NBD}, the lifetime distribution (Fig. 4 *B*, *Right*) indicates

that the side chain is in a more hydrophobic environment, which contradicts current understanding, which presumes a disordered, water-exposed C-terminal tail. Unexpectedly, despite being the narrowest distribution, the distribution of $Y136C_{NBD}$ is best fit with two Gaussian functions with peak maxima at 2.6 and 3.2 ns that are longer than that observed in the presence of micelles (Fig. 4 *B*, *Right*). This result implies that like $V26C_{NBD}$, there are also at least two membrane-associated conformers of $Y136C_{NBD}$.

The power of our coupled approach of using environmentally sensitive NBD and time-resolved fluorescence is reiterated by the comparison of images obtained through total intensity and the NBD decay kinetics measured at specified locations (Fig. 4*C* and *SI Appendix*, Figs. S12–S14). While spatially informative of the location of the protein, differences between individual spots are completely obscured in the intensity-based images (Fig. 4 *C*, *Left*). It is evident that NBD fluorescence decays vary at different puncta, indicative of variations of local environments, plausibly representing influences of specific lipids and/or proteins at exocytic areas (Fig. 4 *C*, *Right*). Moreover, while $V26C_{NBD}$ is anticipated to exhibit heterogeneous behavior based on its broad distribution (Fig. 4*A*), both $V40C_{NBD}$ and $Y136C_{NBD}$ also experience complex environments as evidenced by the presence of long and short NBD fluorescence decay curves at different locations. Intriguingly, all three NBD fluorophores can be found in a water-exposed state as they exhibited short lifetimes at some puncta (Fig. 4*C*, gray curves; τ_{avg} = 0.7 to 1.6 ns; *SI Appendix*, Table S3), reminiscent of soluble α-syn. Additionally, $Y136C_{NBD}$ is observed as having slower decays (Fig. 4*C*; blue curve; τ_{avg} = 2.7 ns), similar to those shown by $V26C_{NBD}$ in the presence of LPC micelles. These observations, which are not apparent in the global distributions, are only revealed by careful measurements at the individual regional level. Although corresponding to rare events, it is clear that membrane-bound α-syn is much more conformationally dynamic than previously realized. This complexity with which α-syn interacts with lipid membranes is only captured through the use of cellularly derived, functionally relevant membranes.

Discussion

The physiological function of α-syn remains poorly understood; however, membrane interactions are imperative to its proposed functions involving synaptic vesicle transmission and homeostasis. Here, we provide insights into the spatial localization of α-syn on the cytosolic membrane that is modulated by lipid/protein complexes pertinent to its function in exocytosis, revealing unexpected protein conformational behavior that challenges the current structural models of membrane-bound α-syn. By using unroofed cells, which encapsulate cellular membrane complexity and topology, we demonstrate that α-syn prefers binding to GM1-rich liquid-ordered lipid domains, which has not been documented before. As both GM1 and α-syn can stabilize and induce positive curvature in the plasma membrane, the spatial enrichment of both entities would prime the plasma membrane for vesicle fusion during exocytosis. As this process is largely driven by membrane curvature (31) and native protein–protein interactions that only exist on intact plasma membranes, recruitment of α-syn to these lipids would be abrogated in giant unilamellar vesicles (29), the prevalent model for evaluating protein partitioning between fluid and liquid-ordered phases. Clearly, simple membrane mimics are not sufficient as α-syn is proven to be extremely sensitive to a variety of membrane properties, including fluidity, curvature, packing defects, and surface charge.

α-Syn is reported to directly promote SNARE complex assembly (2, 56), and further, membrane-bound Rab3a can facilitate α-syn binding to synaptic vesicles (57). Both recruitment of specific lipids and presynaptic proteins such as α-syn may be necessary to either stabilize or induce membrane curvature (52), which needs to be tightly regulated during exocytosis. Conclusively, we show localization of α-syn with proteins (Rab3a, syntaxin-1A, and VAMP2) involved in exocytic vesicle docking and fusion, providing direct evidence of α-syn recruitment at exocytic vesicles on the inner plasma membrane.

Direct spatial observation of conformational heterogeneity of α-syn at the residue level on the cytoplasmic membrane was achieved by NBD lifetime imaging. Unexpectedly, $V26C_{NBD}$ is more sensitive to the lipid environment compared to that of $V40C_{NBD}$, which contradicts experiments performed with synthetic membrane models. In addition, $V26C_{NBD}$ experiences the most heterogeneous environment of the sites investigated, which is counterintuitive as the N terminus is thought to be the membrane anchor, which would then be expected to adopt a well-folded, helical conformation. This inconsistency could be partly due to the fact that the structural models were determined using disordered lipids, which are disparate from the more ordered lipid environments at exocytic sites. Additionally, we reason that in order to accommodate the presence of numerous other proteins at the presynaptic plasma membrane, α-syn may only need to interact with lipids through fewer stretches of amino acids by adopting different local conformations as there are limited free areas for binding. Therefore, while the N-terminal region may have a high affinity for lipid membranes, the generalized α-helical conformation is perturbed by native biomolecules and could be modulated by specific protein–protein interactions. Because exocytic events are highly dynamic, involving coordination between both lipids and proteins, the equilibrium will shift between different α-syn conformations.

Generally, the C terminus of α-syn is thought to remain disordered in solution and thus minimally influences its membrane binding properties. However, our results presented here suggest otherwise. Data clearly indicate that the C terminus interacts with lipids, particularly with zwitterionic phospholipids, as indicated by the increase in fluorescence lifetime in the presence of LPC micelles. This observation is further substantiated on unroofed cells, suggesting that the C terminus could mediate lipid and/or protein interactions at the plasma membrane, related to its exocytic function.

Collectively, our results show that α-syn is more conformationally dynamic at the membrane interface than previously appreciated. We speculate that this inherent plasticity could also make the protein more susceptible to oligomerization at the membrane interface. It still remains unclear whether α-syn oligomerization plays a physiological role in assisting SNARE complex fusion as previously suggested (56) or potentially leads to the pathology of Parkinson's disease by facilitating amyloid fibril formation (58, 59). Nevertheless, under disease-related conditions where α-syn accumulates in the cytosol, there would be an equilibrium shift and a reduction of its activity on the membrane, resulting in deterioration of neuronal function. Therefore, understanding α-syn conformational switching is of importance for future work; fluorescence resonance energy transfer experiments on unroofed cells (60) would be extremely informative in determining the conformational state of membrane-bound α-syn.

In conclusion, we show that α-syn prefers GM1-rich lipid domains and adopts a collection of diverse membrane-bound conformations in order to carry out its function at exocytic sites. These insights were only possible through the coupled approaches of using unroofed cells, derivatization of specific residues with the environmentally sensitive NBD fluorophore, and FLIM measurements. We demonstrate that unroofed cells are a suitable and powerful platform for spectroscopic studies that are broadly applicable. Our results with α-syn reaffirm the need to use cellularly derived and biologically relevant membranes for biophysical characterization in developing a molecular understanding of important protein–lipid interactions. We envision further investigations

would provide insights into the conformational switching of α-syn from a physiological to pathological state and would be equally valuable if extended to other amyloidogenic and membrane-associated proteins.

Materials and Methods

Details regarding reagents, proteins, cell culture, methods for immunofluorescence, confocal fluorescence microscopy, lipid vesicle preparation, fluorescence, and CD spectroscopy are provided in *SI Appendix*.

Unroofing Cells. Cells were unroofed following published protocols (34). Briefly, cells plated on #1.5 poly-D-lysine (PDL)-treated glass coverslips (Neuvitro; H-25–1.5-PDL) were transferred into stabilization buffer (30 mM Hepes, 70 mM KCl, 5 mM $MgCl_2$, 3 mM EGTA, pH 7.4) prior to sonication. The sonicator tip (1/8″ tapered microtip; VWR International; 33996-163) was placed ∼4 to 5 mm above the coverslip, and one to two 400-ms pulses at the lowest power setting were applied (Branson Sonifier 450).

Imaging Spectroscopy. Unroofed cells were incubated with NBD-labeled α-syn for 5 min at room temperature, washed with stabilization buffer three times, and immediately after fixed in 2% paraformaldehyde for 20 min and stored at 4 °C. Unroofed cells were imaged using a 100× silicon oil-immersion objective (Olympus; UPLSAPO100XS) on an inverted microscope (Olympus; IX-73) equipped with an imaging spectrograph (Kymera 193i; Andor Oxford Instruments) with a 600 g/mm grating. The 488-nm line of an Ar-ion laser (Modu-Laser) was pass through a laser clean-up filter and directed to the sample using a 488-nm dichroic. To remove residual excitation light, a 488-nm long-passed emission filter was used. Each image and spectrum was acquired using 5-s exposure time and 10 accumulations with a slit width of 500 μm.

FLIM Measurements. Unroofed cells were prepared as described above. FLIM was carried out using a PicoQuant MicroTime 200 time-resolved confocal fluorescence microscope. The setup consists of an inverted Olympus IX-83 microscope equipped with a 60× water-immersion objective (Olympus; UPLSAPO60XW). NBD-labeled α-syn was excited using a 485-nm pulsed laser operating at a repetition rate of 16 MHz. The excitation light was guided to the sample by a 3-mm multiband-dichroic mirror 405/488. After passing a 100-μm pinhole and a 488-nm long-pass filter, the fluorescence was collected by a PMA Hybrid40 detector (PicoQuant). Images were collected with an integration time of 5 μs at each pixel. For soluble-, micelle- and vesicle-bound NBD-α-syn, time-correlated single-photon counting decays were acquired in point time trace mode with an average photon count greater than 10,000 counts. Images and decay curves were processed and fit using the SymPhoTime 64 software (PicoQuant).

Data Availability. All data are made available within the article or *SI Appendix*.

ACKNOWLEDGMENTS. This work was supported by the Intramural Research Program at the NIH, National Heart, Lung, and Blood Institute (NHLBI). Parts of this research were performed on instruments maintained by the NHLBI Biochemistry (liquid chromatography–mass spectrometry), Biophysics (CD, dynamic light scattering), and Light Microscopy (fluorescence recovery after photobleaching experiments) Cores. We thank Dr. Kem Sochacki and Brigette Heine for providing technical advice and helpful discussions.

1. F. Cheng, G. Vivacqua, S. Yu, The role of α-synuclein in neurotransmission and synaptic plasticity. *J. Chem. Neuroanat.* **42**, 242–248 (2011).
2. J. Burré *et al.*, α-Synuclein promotes SNARE-complex assembly in vivo and in vitro. *Science* **329**, 1663–1667 (2010).
3. D. E. Cabin *et al.*, Synaptic vesicle depletion correlates with attenuated synaptic responses to prolonged repetitive stimulation in mice lacking α-synuclein. *J. Neurosci.* **22**, 8797–8807 (2002).
4. D. Snead, D. Eliezer, Intrinsically disordered proteins in synaptic vesicle trafficking and release. *J. Biol. Chem.* **294**, 3325–3342 (2019).
5. D. Eliezer, E. Kutluay, R. Bussell Jr., G. Browne, Conformational properties of α-synuclein in its free and lipid-associated states. *J. Mol. Biol.* **307**, 1061–1073 (2001).
6. W. S. Davidson, A. Jonas, D. F. Clayton, J. M. George, Stabilization of α-synuclein secondary structure upon binding to synthetic membranes. *J. Biol. Chem.* **273**, 9443–9449 (1998).
7. E. Jo, J. McLaurin, C. M. Yip, P. St George-Hyslop, P. E. Fraser, α-Synuclein membrane interactions and lipid specificity. *J. Biol. Chem.* **275**, 34328–34334 (2000).
8. B. Fauvet *et al.*, α-Synuclein in central nervous system and from erythrocytes, mammalian cells, and *Escherichia coli* exists predominantly as disordered monomer. *J. Biol. Chem.* **287**, 15345–15364 (2012).
9. C. C. Jao, B. G. Hegde, J. Chen, I. S. Haworth, R. Langen, Structure of membrane-bound α-synuclein from site-directed spin labeling and computational refinement. *Proc. Natl. Acad. Sci. U.S.A.* **105**, 19666–19671 (2008).
10. E. R. Georgieva, T. F. Ramlall, P. P. Borbat, J. H. Freed, D. Eliezer, Membrane-bound α-synuclein forms an extended helix: Long-distance pulsed ESR measurements using vesicles, bicelles, and rodlike micelles. *J. Am. Chem. Soc.* **130**, 12856–12857 (2008).
11. G. Fusco *et al.*, Structural basis of synaptic vesicle assembly promoted by α-synuclein. *Nat. Commun.* **7**, 12563 (2016).
12. Z. Zhang *et al.*, Calcium accelerates SNARE-mediated lipid mixing through modulating α-synuclein membrane interaction. *Biochim. Biophys. Acta Biomembr.* **1860**, 1848–1854 (2018).
13. J. Diao *et al.*, Native α-synuclein induces clustering of synaptic-vesicle mimics via binding to phospholipids and synaptobrevin-2/VAMP2. *eLife* **2**, e00592 (2013).
14. J. Sun *et al.*, Functional cooperation of α-synuclein and VAMP2 in synaptic vesicle recycling. *Proc. Natl. Acad. Sci. U.S.A.* **116**, 11113–11115 (2019).
15. T. S. Ulmer, A. Bax, N. B. Cole, R. L. Nussbaum, Structure and dynamics of micelle-bound human α-synuclein. *J. Biol. Chem.* **280**, 9595–9603 (2005).
16. S. B. Lokappa, T. S. Ulmer, α-Synuclein populates both elongated and broken helix states on small unilamellar vesicles. *J. Biol. Chem.* **286**, 21450–21457 (2011).
17. S. Chandra, X. Chen, J. Rizo, R. Jahn, T. C. Südhof, A broken α-helix in folded α-synuclein. *J. Biol. Chem.* **278**, 15313–15318 (2003).
18. T. Das, D. Eliezer, Membrane interactions of intrinsically disordered proteins: The example of α-synuclein. *Biochim. Biophys. Acta. Proteins Proteomics* **1867**, 879–889 (2019).
19. C. M. Pfefferkorn, Z. Jiang, J. C. Lee, Biophysics of α-synuclein membrane interactions. *Biochim. Biophys. Acta* **1818**, 162–171 (2012).
20. M. M. Ouberai *et al.*, α-Synuclein senses lipid packing defects and induces lateral expansion of lipids leading to membrane remodeling. *J. Biol. Chem.* **288**, 20883–20895 (2013).
21. J. Varkey *et al.*, Membrane curvature induction and tubulation are common features of synucleins and apolipoproteins. *J. Biol. Chem.* **285**, 32486–32493 (2010).
22. Z. Jiang, M. de Messieres, J. C. Lee, Membrane remodeling by α-synuclein and effects on amyloid formation. *J. Am. Chem. Soc.* **135**, 15970–15973 (2013).
23. N. Mizuno *et al.*, Remodeling of lipid vesicles into cylindrical micelles by α-synuclein in an extended α-helical conformation. *J. Biol. Chem.* **287**, 29301–29311 (2012).
24. C. Eichmann *et al.*, Preparation and characterization of stable α-synuclein lipoprotein particles. *J. Biol. Chem.* **291**, 8516–8527 (2016).
25. J. Varkey *et al.*, α-Synuclein oligomers with broken helical conformation form lipoprotein nanoparticles. *J. Biol. Chem.* **288**, 17620–17630 (2013).
26. L. Kjaer, L. Giehm, T. Heimburg, D. Otzen, The influence of vesicle size and composition on α-synuclein structure and stability. *Biophys. J.* **96**, 2857–2870 (2009).
27. E. R. Middleton, E. Rhoades, Effects of curvature and composition on α-synuclein binding to lipid vesicles. *Biophys. J.* **99**, 2279–2288 (2010).
28. M. B. Jensen *et al.*, Membrane curvature sensing by amphipathic helices: A single liposome study using α-synuclein and annexin B12. *J. Biol. Chem.* **286**, 42603–42614 (2011).
29. M. Stöckl, P. Fischer, E. Wanker, A. Herrmann, α-Synuclein selectively binds to anionic phospholipids embedded in liquid-disordered domains. *J. Mol. Biol.* **375**, 1394–1404 (2008).
30. B. Nuscher *et al.*, α-Synuclein has a high affinity for packing defects in a bilayer membrane: A thermodynamics study. *J. Biol. Chem.* **279**, 21966–21975 (2004).
31. E. I. O'Leary, Z. Jiang, M. P. Strub, J. C. Lee, Effects of phosphatidylcholine membrane fluidity on the conformation and aggregation of N-terminally acetylated α-synuclein. *J. Biol. Chem.* **293**, 11195–11205 (2018).
32. P. J. Quinn, C. Wolf, The liquid-ordered phase in membranes. *Biochim. Biophys. Acta* **1788**, 33–46 (2009).
33. D. L. Fortin *et al.*, Lipid rafts mediate the synaptic localization of α-synuclein. *J. Neurosci.* **24**, 6715–6723 (2004).
34. J. Heuser, The production of "cell cortices" for light and electron microscopy. *Traffic* **1**, 545–552 (2000).
35. P. B. Ghosh, M. W. Whitehouse, 7-Chloro-4-nitrobenzo-2-oxa-1,3-diazole: A new fluorigenic reagent for amino acids and other amines. *Biochem. J.* **108**, 155–156 (1968).
36. L. A. Shepard *et al.*, Identification of a membrane-spanning domain of the thiol-activated pore-forming toxin *Clostridium perfringens* perfringolysin O: An α-helical to β-sheet transition identified by fluorescence spectroscopy. *Biochemistry* **37**, 14563–14574 (1998).
37. S. Mukherjee, A. Chattopadhyay, A. Samanta, T. Soujanya, Dipole-moment change of NBD group upon excitation studied using solvatochromic and quantum-chemical approaches—implications in membrane research. *J. Phys. Chem.* **98**, 2809–2812 (1994).
38. A. M. Powl, J. N. Wright, J. M. East, A. G. Lee, Identification of the hydrophobic thickness of a membrane protein using fluorescence spectroscopy: Studies with the mechanosensitive channel MscL. *Biochemistry* **44**, 5713–5721 (2005).
39. T. Pan, J. Zhu, W. J. Hwu, J. Jankovic, The role of α-synuclein in melanin synthesis in melanoma and dopaminergic neuronal cells. *PLoS One* **7**, e45183 (2012).
40. G. Scott, Q. Zhao, Rab3a and SNARE proteins: Potential regulators of melanosome movement. *J. Invest. Dermatol.* **116**, 296–304 (2001).
41. K. Simons, E. Ikonen, Functional rafts in cell membranes. *Nature* **387**, 569–572 (1997).
42. K. Simons, D. Toomre, Lipid rafts and signal transduction. *Nat. Rev. Mol. Cell Biol.* **1**, 31–39 (2000).
43. S. Izuta *et al.*, Microfluidic preparation of anchored cell membrane sheets for in vitro analyses and manipulation of the cytoplasmic face. *Sci. Rep.* **7**, 14962 (2017).

44. C. M. Pfefferkorn, J. C. Lee, Tryptophan probes at the α-synuclein and membrane interface. *J. Phys. Chem. B* **114**, 4615–4622 (2010).
45. C. M. Pfefferkorn *et al*., Depth of α-synuclein in a bilayer determined by fluorescence, neutron reflectometry, and computation. *Biophys. J.* **102**, 613–621 (2012).
46. C. R. Bodner, C. M. Dobson, A. Bax, Multiple tight phospholipid-binding modes of α-synuclein revealed by solution NMR spectroscopy. *J. Mol. Biol.* **390**, 775–790 (2009).
47. A. Ohrfelt *et al*., Identification of novel α-synuclein isoforms in human brain tissue by using an online nanoLC-ESI-FTICR-MS method. *Neurochem. Res.* **36**, 2029–2042 (2011).
48. R. G. Parton, Ultrastructural localization of gangliosides; GM1 is concentrated in caveolae. *J. Histochem. Cytochem.* **42**, 155–166 (1994).
49. M. Bastiani, R. G. Parton, Caveolae at a glance. *J. Cell Sci.* **123**, 3831–3836 (2010).
50. A. J. Trexler, K. A. Sochacki, J. W. Taraska, Imaging the recruitment and loss of proteins and lipids at single sites of calcium-triggered exocytosis. *Mol. Biol. Cell* **27**, 2423–2434 (2016).
51. K. A. Sochacki, A. M. Dickey, M. P. Strub, J. W. Taraska, Endocytic proteins are partitioned at the edge of the clathrin lattice in mammalian cells. *Nat. Cell Biol.* **19**, 352–361 (2017).
52. E. Lauwers, R. Goodchild, P. Verstreken, Membrane lipids in presynaptic function and disease. *Neuron* **90**, 11–25 (2016).
53. Z. Jiang, S. K. Hess, F. Heinrich, J. C. Lee, Molecular details of α-synuclein membrane association revealed by neutrons and photons. *J. Phys. Chem. B* **119**, 4812–4823 (2015).
54. J. Madine, A. J. Doig, D. A. Middleton, A study of the regional effects of α-synuclein on the organization and stability of phospholipid bilayers. *Biochemistry* **45**, 5783–5792 (2006).
55. G. Fusco *et al*., Direct observation of the three regions in α-synuclein that determine its membrane-bound behaviour. *Nat. Commun.* **5**, 3827 (2014).
56. J. Burré, M. Sharma, T. C. Südhof, α-Synuclein assembles into higher-order multimers upon membrane binding to promote SNARE complex formation. *Proc. Natl. Acad. Sci. U.S.A.* **111**, E4274–E4283 (2014).
57. R. H. Chen *et al*., α-Synuclein membrane association is regulated by the Rab3a recycling machinery and presynaptic activity. *J. Biol. Chem.* **288**, 7438–7449 (2013).
58. C. Galvagnion, The role of lipids interacting with α-synuclein in the pathogenesis of Parkinson's disease. *J. Parkinsons Dis.* **7**, 433–450 (2017).
59. E. I. O'Leary, J. C. Lee, Interplay between α-synuclein amyloid formation and membrane structure. *Biochim. Biophys. Acta. Proteins Proteomics* **1867**, 483–491 (2019).
60. S. E. Gordon, M. Munari, W. N. Zagotta, Visualizing conformational dynamics of proteins in solution and at the cell membrane. *eLife* **7**, e37248 (2018).